Journal of the European Ceramic Society 21 (2001) 269–275

www.elsevier.com/locate/jeurceramsoc

Residual stresses and R-curve behavior of AlN/Mo composite

Orfeo Sbaizero [a,*], Giuseppe Pezzotti [b]

[a] *Department of Materials Engineering, University of Trieste, Via Valerio 2, 34127 Trieste, Italy*
[b] *Department of Materials, Kyoto Institute of Technology, Matsugasaki, Sakyo-ku, Kyoto 606-8585, Japan*

Received 25 May 2000; accepted 2 August 2000

Abstract

AlN matrix was added with different amounts of metal molybdenum particles. R-curves were measured during stable crack propagation and a piezo-spectroscopic technique has been used to assess both, the residual stresses in the AlN matrix and the bridging stresses developed along the crack wake (at the metal/matrix interface) at the critical condition for crack propagation. Thermal residual stresses were compressive for Mo fractions $\leqslant 15\%$; they were ≈ 0 when 20 vol.% of Mo was added and tensile for fractions $\geqslant 30$ vol.%. These stresses affected the composites toughness in two ways: (i) compressive residual stresses in the AlN matrix slightly enhanced the critical stress intensity factor for crack initiation, K_{I0}, of the composite, (ii) tensile residual stresses weakened the metal/ceramic interface, leading to an enbrittlement of the composite. For Mo $\leqslant 20\%$, metal particles bridged the crack whereas when 30 vol.% of Mo was present the metal/ceramic interface was weakened and became the most favorable site for fracture of the bridging sites. As a result the toughness of the composite was strongly reduced. The theoretical R-curves calculated from the average (microscopic) bridging stress distribution obtained by in situ Raman spectroscopy were in good agreement with the experimental data.

Keywords: AlN–Mo; Composites; Mechanical properties; R-curves; Residual stresses

1. Introduction

Trends in electronic device manufacture and applications indicate that substrates having high thermal conductivity will become of increasing importance.[1,2] The most commonly used substrates are alumina (Al_2O_3) or even better, as far as the thermal conductivity, long term corrosion and radiation resistances are concerned, aluminum nitride (AlN). The latter material also has several of other physical properties that make it interesting for applications in microcircuit packaging: a thermal expansion coefficient (CTE) close to that of silicon, a high electrical resistivity and a moderately low dielectric constant. Unfortunately, as usual for ceramic materials, its actual application is primarily limited because of the low fracture toughness and thermal shock resistance. Attempts have been made to improve the fracture toughness of ceramics adding a dispersed ductile metallic second phase.[3–7] Among metals, a refractory ductile phase with high thermal conductivity might represent the ideal choice as toughening agent.

Although molybdenum cannot be considered to be a very ductile metal, it is chemically compatible with the AlN matrix and has greater ductility, potentially leading to a toughness increase in the composites. Experimental studies[8–10] have shown that the primary mechanism responsible for the enhanced toughness of ceramic/metal composites is the elasto-plastic bridging across the crackpath, operated by intact metal ligaments. Although the toughening mechanisms in ceramics containing metallic dispersions have been studied in some detail, very little work has been done to elucidate how some factors like CTE- and elastic moduli-mismatch can affect the overall composite performance.

In this paper, a Mo metal dispersion is added to AlN ceramic matrix. Residual stresses produced on cooling from sintering temperature due to mismatch in thermo-mechanical properties between ceramic and metal are assessed by piezo-spectroscopy techniques.[11] Then, the effect of these residual stresses on the toughness behavior of the composite will be examined by in situ fracture experiments and discussed.

* Corresponding author.
E-mail address: sbaizero@univ.trieste.it (O. Sbaizero).

0955-2219/01/$ - see front matter
PII: S0955-2219(00)00204-1

2. Experimental procedures

2.1. Materials

Increasing amounts (10, 15, 20 and 30 vol.%) of molybdenum powder (Japan New Metals Co., Japan; average particle size = 1.56 μm) were mixed with AlN powder (Tokuyama Soda, Ltd., Japan). The ceramic–metal powder mixtures were attrition milled in isopropyl alcohol for 4 h. After drying, samples of each composite were pre-formed by uniaxial pressing followed by cold isostatic pressing at 100 MPa. Hot-pressing was then performed in a graphite die with its inner walls coated with a BN slurry to avoid any interaction between the specimens and the graphite die. For all the composites, the maximum hot-pressing pressure was 30 MPa. The selected sintering temperature and time were 1700°C and 1 h, respectively. The samples were then slowly cooled down (200°C/h) to room temperature. Hot-pressed samples were in the form of discs with diameter and thickness of 50 and 10 mm, respectively. The density, measured by the Archimedes method, was >96.5% of its theoretical value calculated from the rule of mixtures. The average grain size of the matrices, assessed by image analysis from scanning electron micrographs, was in the range of 3–5 μm, while the average grain size of the Mo particles after hot pressing was in the range 8–12 μm for all the composites investigated.

2.2. Fracture mechanics characterization

Hot-pressed discs were cut in the form of rectangular bars for fracture mechanics tests with dimensions 3×4×20 mm (breadth, B; width, W; length, L). A straight-through notch with a relative depth, $a/W = 0.5$ was introduced at the center of the fracture mechanics specimen by a diamond blade (thickness = 0.15 mm). Then, to reduce the influence of a finite notch-tip radius, the bottom part of the saw-notch was sharpened with a razor blade sprinkled with fine diamond paste. Using this procedure the notch root was sharpened to a radius <5 μm. To achieve stable fracture propagation, in bending geometry, the crack stabilizer designed by Nojima and Nakai[12] for a three-point bending geometry was used (span = 16 mm). The load–displacement relation was directly measured with semiconductor strain gauges placed both on the loading bar and on the tensile surface of the specimen. Further details of the notching procedure and the bending stabilizer geometry have been reported elsewhere.[13,14] R-curve data were collected from the load–displacement curves obtained under the relatively fast cross-head speed 0.1 mm/min. The crack length was measured upon crack arrest by scanning electron microscopy at various stages of crack propagation. The crack resistance value, K_R, as a function of crack extension, Δa, was calculated from standard equations. The maximum crack extension which could be monitored in the present bending geometry was ≈800 μm.

2.3. Raman spectroscopy

The determination of stresses by Raman spectroscopy is based on the piezo-spectroscopy effect, involving a spectral shift due to the applied stress.[15] The technique, applied to determine microscopic stresses in ceramic materials, and its accuracy have been already described in previous works.[10,11] The Raman spectroscopic apparatus used was an ISA, T 64000 from Jovin-Yvon. An Ar-ion laser operating at a wavelength of 488 nm with a power of 300 mW was used as the excitation source, while an optical microscope was used both to focus the laser on the sample and to collect the scattered light. Light frequencies were analyzed using a triple monochromator equipped with a charge-coupled device (CCD) camera. The spatial resolution used for residual stress measurements in the Raman apparatus was ≅10 μm. The penetration depth of the laser beam below the specimen surface was estimated to be between 10 and 20 μm.

In the crack-profile maps experiments, a three-point bend loading jig was equipped with a load cell of 100 N and placed into the Raman apparatus. Profiles of stable propagating cracks were monitored in situ by optical microscopy. At the same time, Raman spectra were recorded in the matrix, near the ceramic/metal interface of bridging sites, both at zero external load and at the critical load for crack propagation. Since a large number of points had to be recorded under the same applied load, the load was temporarily kept constant. However, no significant load–relaxation over such a holding time could be monitored. In these mapping experiments the dimension of the laser spot on the sample was ≅5 μm. To single out the actual bridging effect without the influence of local residual stress, a linear map of Raman spectra was recorded along the crack profile at zero external load. This map was used to establish the local "zero-stress" values of the Raman peak frequency. Then, a linear map was collected at the same locations along the crack, but with the external load at the onset value for crack propagation. The neat (local) peak shifts were then calculated by subtracting at any location the frequency recorded at zero external load from that recorded at the onset load for fracture. The collected Raman data were analyzed with the curve-fitting algorithms included in the SpectraCalc software package (Galactic Industries Corp.). Local stresses at the monitored locations were calculated from the respective frequency shifts according to the piezo-spectroscopic coefficient. The average uniaxial piezo-spectroscopic coefficient $\Pi_u = -1.8\ \mathrm{cm^{-1}\ GPa^{-1}}$, determined in a previous work,[16] was employed to linearly relate the frequency shift ($\Delta\nu$) to the uniaxial bridging stress (σ_{BR})

according to the relation ($\sigma_{BR} = \Pi_u \Delta\nu$). On the other hand, the residual triaxial state of stress due to thermal expansion and elastic mismatches between the metal and ceramic phases was evaluated using an average hydrostatic piezo-spectroscopy coefficient, $\Pi_t \cong 3\Pi_u$, which neglects the anisotropy effect on the piezo-spectroscopic tensor of AlN.

3. Results

Microstructures of the hot-pressed composites are shown in Fig. 1. As can be seen, the distribution of the Mo particles is relatively uniform for Mo amounts <20 vol.%. In these composites, the attrition milling process did not significantly change the initial particle size distribution of the Mo powders, and the average particle size in the sintered composites was always close to ≈ 8 μm. When the amount of the Mo phase was 30 vol.%, formation of Mo clusters was observed and the average metal particle size reached ≈ 12 μm.

The experimental average residual stresses in the AlN matrix as measured by Raman spectroscopy is reported as a function of the Mo addition in Table 1. In AlN/Mo composites, the thermal expansion coefficient of the metal is only slightly higher compared to that of the matrix, therefore the residual stress should be of relatively low magnitude and compressive in the ceramic matrix. The experimental residual stress in AlN/Mo was indeed compressive when 10 and 15% of Mo was added, however it was ≈ 0 for 20 vol.% of Mo and became tensile for 30 vol.% Mo addition.

The experimental R-curve behavior of the composites is plotted in Fig. 2, which shows the dependence of crack resistance, K_R, upon the crack extension, Δa, from the root of the notch. The K_R value plotted at $\Delta a = 0$ (usually indicated as K_{I0}) is that corresponding to the load at which the load–displacement curve diverges from a linear trend. This value increased of almost 25% as the amount of the dispersoid increased going from 2.2 MPa $\sqrt{m}$ (10 vol.% of Mo addition) to 2.75 MPa $\sqrt{m}$ (20 vol.% of Mo addition). However, despite the larger fraction of metallic phase addition of 30 vol.% Mo produced an embrittlement of the composite (i.e. $K_{I0} \approx 2.35$ MPa $\sqrt{m}$).

Typical linear maps of the bridging stresses as a function of the abscissa x' along the crack (with origin at the crack tip) are shown in Fig. 3(a–d) as a function

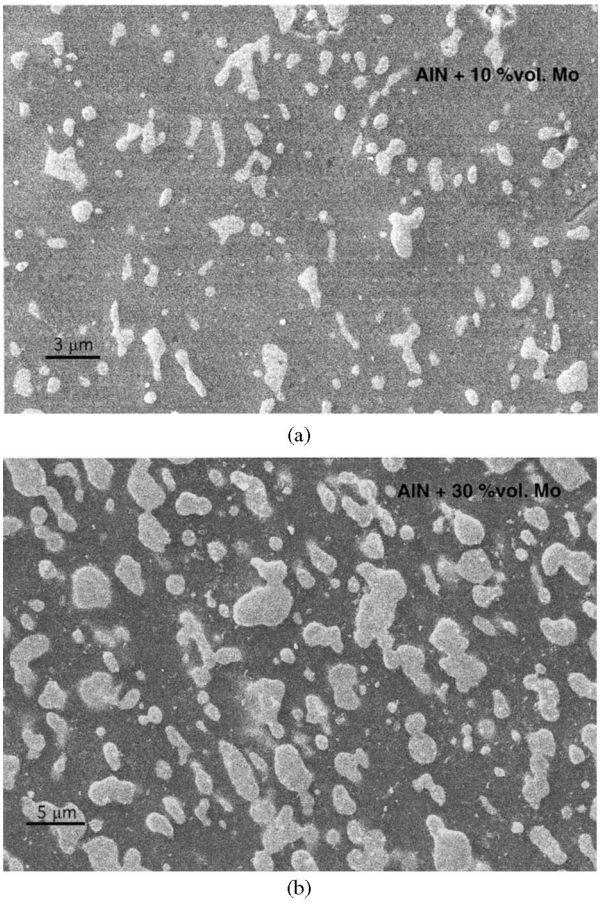

Fig. 1. Microstrucures of AlN/Mo composites after hot-pressing, (a) 10 vol.% of Mo, (b) 30 vol.% of Mo.

Table 1
Residual and bridging stresses in the AlN/Mo composites

Composite	Residual stress (MPa)	Average bridging stress (MPa)
AlN/Mo (10 vol.%)	−57	42
AlN/Mo (15 vol.%)	−41	71
AlN/Mo (20 vol.%)	12	88
AlN/Mo (30 vol.%)	200	48

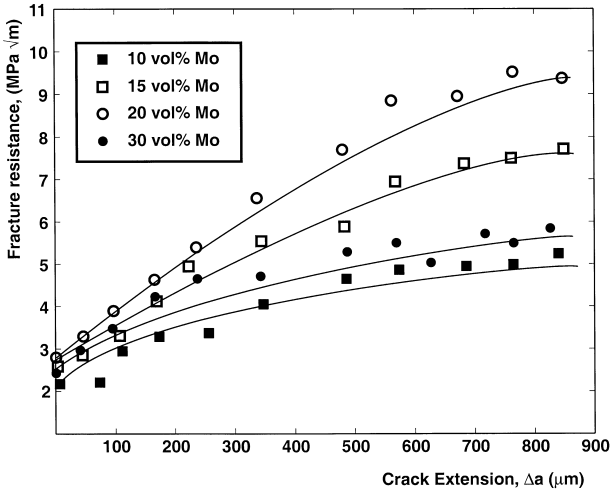

Fig. 2. Experimental data and theoretical assessments from microscopic briding stress data of rising R-curve behavior in AlN/Mo composites.

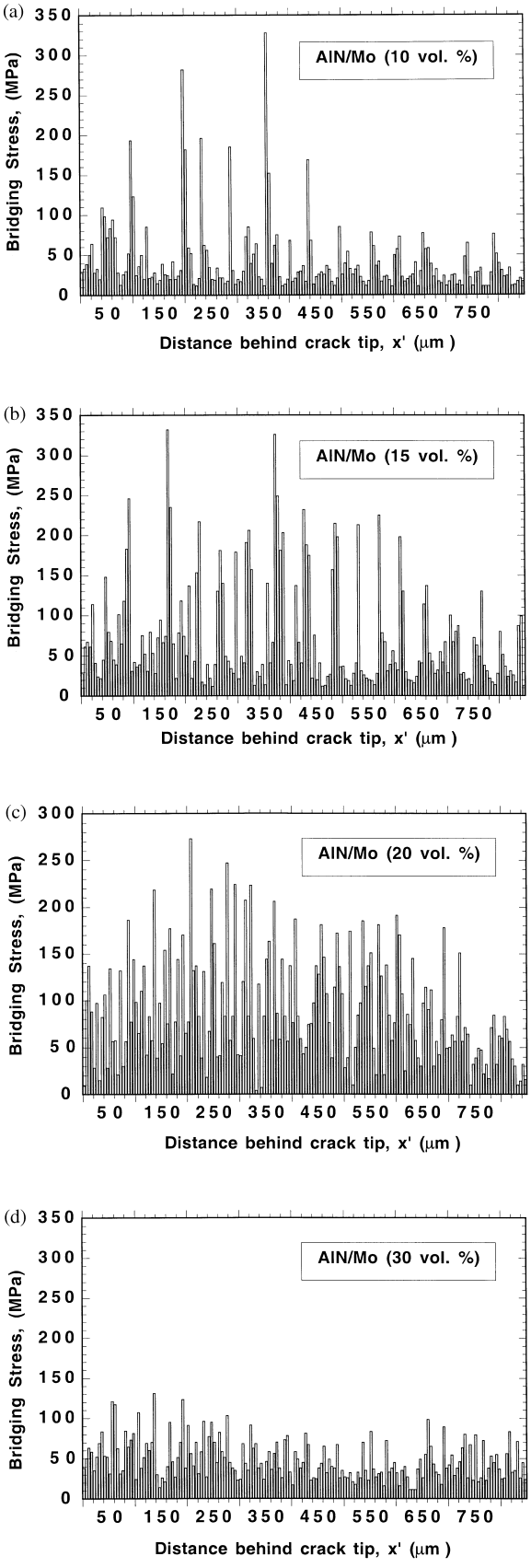

Fig. 3. Typical linear map of the bridging stresses as a function of the distance from the crack tip for: (a) 10 vol.%, (b) 15 vol.%, (c) 20 vol.% and (d) 30 vol.% of Mo.

of the Mo dispersoids volume fraction. In the composites with 10, 15 and 20 vol.%, of Mo addition, maximum bridging stresses as high as 300 MPa were measured, although the bridging sites showing such a high bridging stress were relatively few. Therefore the resulting average stress (i.e. = 42, 71, and 88 MPa for 10, 15 and 20 vol.% of Mo, respectively). On the other hand, the bridging stress map for the composite with 30 vol.% of Mo showed quite different features. Local stresses never exceed 150 MPa, although the average stress, 48 MPa, was higher than that of the composite added with 10 vol.% of Mo. The rationale for the dependence of bridging stress on the Mo fraction can be found by observing the crack propagation path by SEM. For low fractions, Mo particles were systematically observed to bridge the crack profile up to their fracture (with few experimental evidence of metal plasticity) (Fig. 4a). On the other hand, when 30 vol.% Mo

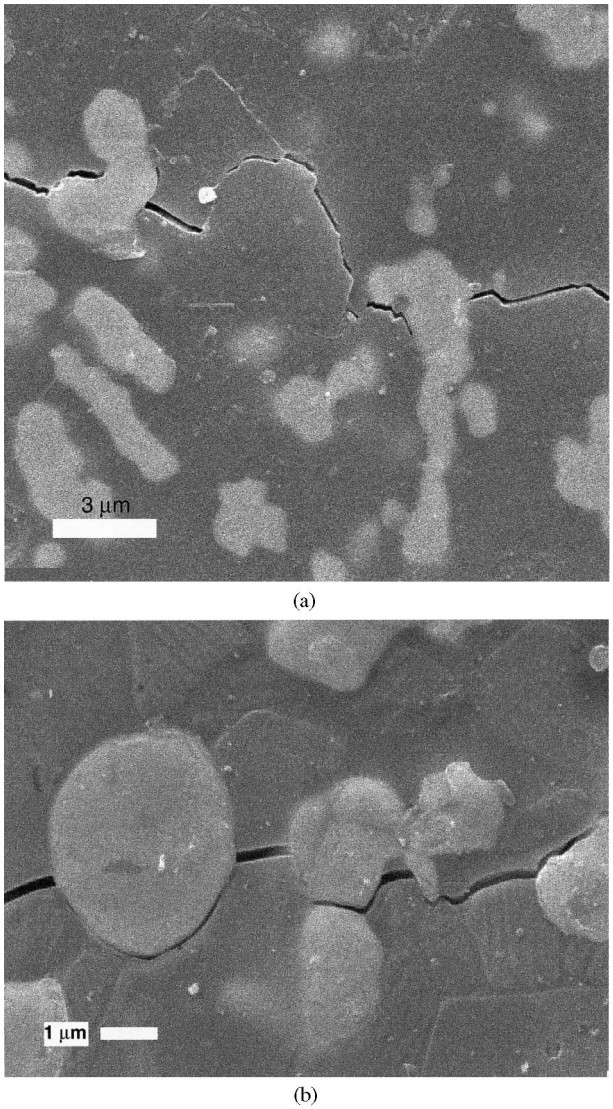

Fig. 4. Typical crack propagation paths for: (a) AlN/15 vol.% Mo, and (b) AlN/30 vol.% Mo.

was added, a weak metal/ceramic interface was observed, the interface itself becoming the most favorable path for crack propagation (Fig. 4b).

4. Discussion

Fracture mechanics studies[17,18] have shown that, independent of the morphology of the metal phase (i.e. isolated inclusions or continuous network through the composites), the main toughening mechanism, in metal-dispersed ceramics, arises from a bridging effect operated by metallic ligaments stretched behind the crack tip, until they break. Indeed also in the present composites, bridging metal ligaments were observed in the crack wake (Fig. 4). However, residual stresses can change the local state of stress at the matrix/dispersoid interface, affecting in this way the maximum bridging stresses carried out by the metal ligaments, and therefore the resulting rising R-curve. Depending on the sign of localized residual stresses, the crack path can be attracted or repelled by the metal particles. When the particles have a higher CTE as well as a higher elastic modulus than the matrix, theory predicts that crack has a tendency to propagate around the particles, and bridging can not occur.[19] At high fractions of dispersoids the thermal residual stress in ceramic-matrix composites may become strongly dependent on the volume fraction of the added particles. Indeed, Virkar and Johnson[20] postulated a periodic tension-compression residual stress field whose magnitude depends on the CTE mismatch between the constituent. These researchers showed that the thermal residual stresses in the composite depend not only on the CTE mismatch and the "stress freezing" temperature interval, ΔT, but also, and in a substantial way, on the dispersoid/matrix stiffness ratio, their Poisson ratio, the volume fraction and the size of the dispersoid as well as the boundary conditions at dispersoid/matrix interface. The actual stress at any point of the matrix is considered to be the sum of two terms: (i) a uniform average stress, σ_m, related to the elastic constants of the matrix and the dispersoid (Young modulus, Poisson ratio) and, the CTE misfit strain ($\Delta\alpha\ \Delta T$). This stress is an increasing linear function of the dispersoid volume fraction, f; (ii) a locally fluctuating stress developed by neighboring particles, σ_{fl}.[21,22] In this latter case, the value of the residual stress is related also to the dispersoid size and the interparticle distance, which in turn, is proportional to $f^{-1/3}$.

The aforementioned uniform average stress, σ_m is given by:[20]

$$\sigma_m = \frac{2\beta f \Delta T \Delta\alpha E_m}{(1-f)(\beta+2)(1+\nu_m)+3\beta f(1-\nu_m)} \quad (1)$$

where $\Delta\alpha$ is the CTE mismatch, ΔT is the "stress freezing" temperature interval. Given the high refractoriness of the Mo metal phase, ΔT was taken as the difference between the hot-pressing temperature and room temperature, E is the Young modulus, ν the Poisson ratio. The subscripts m and d refer to the matrix and dispersoid, respectively, f is the dispersoid volume fraction and the adimensional constant, β, is given as:

$$\beta = \frac{(1+\nu_d)E_d}{(1-2\nu_m)E_m} \quad (2)$$

The fluctuating stress component is expressed as follows:

$$\sigma_{fl} = \frac{\beta\Delta T\Delta\alpha E_m\left[\dfrac{D}{(\lambda-D)} - \dfrac{D^3}{(2\lambda-D)(\lambda-D^2)}\right]}{2[(1+\nu_m)(\beta+2)]} \quad (3)$$

where D is the dispersoid size and λ is the interparticle distance which, for spherical particles, can be expressed as:[23]

$$\lambda = D\left(\frac{\pi}{6f}\right)^{1/3} \quad (4)$$

When this model is applied to the present AlN/Mo composites, it is found that, despite the relatively low mismatch of thermoelastic properties between the ceramic and metal phases (Table 2) the thermal residual stress field varies appreciably with the metal dispersoid volume fraction. The uniform average stress, σ_m, the locally fluctuating stress σ_{fl}, and the resulting total residual stress $\sigma_{tot}=\sigma_m+\sigma_{fl}$ are plotted in Fig. 5 as a function of the volume fraction of the metal phase. In this plot, the experimental data obtained by piezo-spectroscopy analysis are also shown. A reasonable matching is found between the theoretical model and the experimental data, which show a common trend according to which the total residual stress in the AlN/Mo composites remains slightly compressive at Mo contents <15 vol.% and becomes tensile at $f\geqslant 20$ vol.%. At higher metal contents the total residual stress steeply increases, eventually affecting the strength of the matrix/dispersoid interface. A weakened interface may reduce the bridging action so that the metal ligaments are less effective for toughening.

The R-curve contribution arising from the bridging stress, σ_{br}, can be precisely computed from the knowledge

Table 2
Thermo-elastic properties of the Mo metal dispersoid and the AlN matrix

Material	Young modulus (GPa)	CTE (10^{-6}/K)	Poisson ratio
AlN	320	5	0.25
Mo	340	5.4	0.33

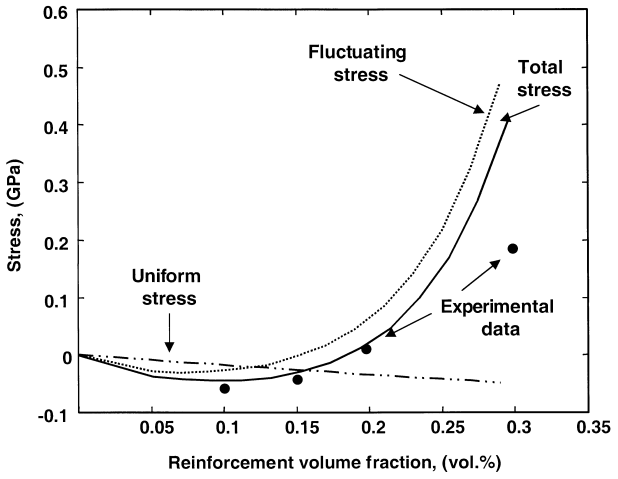

Fig. 5. Uniform, fluctuating and total (average) residual thermal stresses calculated according to the Virkar and Johnson[15] equations, as a function of the volume fraction of Mo added. These theoretical predictions are compared with the experimental residual stress data by piezo-spectroscopy evolution.

of the microscopic bridging stress distribution according to the equation valid for slit cracks:[24]

$$K_R = K_{I0} + \left(\frac{2}{\pi}\right)^{1/2} \sum_{j=0}^{n} \int_{x_j}^{x_{j+1}} \frac{\sigma_{br}(x_j')}{(x')^{1/2}} dx \approx K_{I0} + \left(\frac{2}{\pi}\right)^{1/2} \overline{\sigma_{br}} \int_0^{\Delta a} \frac{dx'}{(x')^{1/2}} \quad (5)$$

where σ_{br} (x′) and $\overline{\sigma_{br}}$ are the discrete bridging stress distribution function and its average value over the crack extension Δa. The variable x', with origin at the crack tip, locates the source point for the bridging stress, σ_{br} (x').

Numerical integration of Eq. (5), performed using the average bridging stress value given in Table 1, leads to the calculated curves reported in Fig. 2. The results of this calculation fit with a good approximation the experimental data, confirming that the main effect on toughening in the AlN/Mo composites is provided by crack-face bridging. For the composites with 20 vol.% of Mo, which showed the highest bridging stresses, the numerical integration over a crack propagation ≈150 μm gives a slight understimation of the experimental data. This discrepancy arises from the approximation of Eq. (5), valid only for relatively short cracks, when used for long cracks (in presence of high bridging stresses).

5. Conclusions

AlN matrix was added with increasing amounts of metal molybdenum and hot-pressed at 1700°C. The room-temperature fracture behavior (i.e. rising R-curve upon stable crack propagation), of these composites was measured and a piezo-spectroscopic technique used to assess both, the average residual stresses in the AlN matrix and the microscopic distribution of bridging stresses by the metal dispersoids across the crack path, at critical condition for fracture propagation. Residual stresses were compressive for Mo fractions $\leqslant 15\%$; they were ≈0 for 20 vol.% of Mo, and became tensile for 30 vol.% Mo addition.

Thermal residual stresses affected the composites toughness in two ways: (i) K_{I0}, slightly increased for $10\% \leqslant f \leqslant 20\%$ Mo from 2.2 to 2.75 MPa $\sqrt{m}$. However a further increase of f to 30% produced embrittlement. (ii) The crack propagation mode was altered by increasing the Mo fraction. For $f \leqslant 20\%$, Mo particles bridge the crack up to their fracture, whereas when 30 vol.% of Mo was present the metal/ceramic interface was weakened and intergranular crack propagation around the Mo particles occured. As a result, in composites containing 10, 15 and 20 vol.% of Mo metal, bridging stresses of relatively high magnitude were measured, resulting in a average bridging stress increase as the amount of Mo increased. The weakened interface in the composite containing 30 vol% of Mo reduced the bridging stress magnitude, thus degradating the rising R-curve behavior of the composite.

The present study confirms the suitability of piezo-spectroscopy techniques in measuring and relating macroscopic and microscopic stress fields in ceramic materials and related composites.

Acknowledgements

One author (O.S.) acknowledges the financial support, for this research, from the Italian National Research Council (CNR) under the grant PF MSTA II.

References

1. Harper, C.A. and Staley, W.W., *Electron. Packaging Prod.*, 58(4) 1985.
2. Simons, R. E., Thermal management of electronic packages. *Solid State Technol*, 1983, **26**(10), 131–137.
3. Kristic, V. D., On the fracture of brittle matrix–ductile particle composites. *Phil. Mag. A*, 1983, **48**(5), 695–708.
4. Thompson, L. R. and Raj, R., In-situ stress–strain response of small metal particles embedded in a ceramic matrix. *Acta Metall. Mater.*, 1994, **42**(7), 2477–2485.
5. Chou, W. B. and Tuan, W. H., Toughening and strengthening of alumina with silver inclusions. *J. Eur. Ceram. Soc.*, 1995, **15**(4), 291–295.
6. Sekino, T. and Niihara, K., Fabrication and mechanical properties of fine-tungsten-dispersed alumina-based composites. *J Mater. Sci.*, 1997, **32**(15), 3943–3949.
7. Bartolome, J. F., Diaz, M., Moya, J. J. and Tomsia, A. P., Mullite/molybdenum ceramic–metal composites. *Acta Mater.*, 1999, **47**(14), 3891–3899.

8. Khan, A. A. and Labbe, J. C., Aluminium nitride molybdenum ceramic matrix composites: influence of molybdenum concentration on the mechanical properties. *J Mater Sci.*, 1997, **32**(14), 3829–3833.
9. Sbaizero, O. and Pezzotti, G., Fracture energy and R-curve behavior of Al_2O_3/Mo composites. *Acta Mater.*, 1998, **46**(2), 681–687.
10. Pezzotti, G., Suenobu, H., Nishida, T. and Sbaizero, O., Measurement of microscopic bridging stresses in alumina/molybdenum composite by in situ fluorescence spectroscopy. *J. Am. Ceram. Soc.*, 1999, **82**(5), 1257–1262.
11. Pezzotti, G. and In situ study of fracture mechanisms in advanced ceramics using fluorescence Raman microprobe spectroscopy, *J. Raman Spectroscopy*, 1999, **30**, 867–875.
12. Nojima, T. and Nakai, O., Stable crack extension of an alumina ceramic in three-point bending test. *J. Soc. Mater. Sci. Jpn*, 1993, **42**(475), 412–418.
13. Nishida, T., Hanaki, Y., Nojima, T. and Pezzotti, G., Measurement of rising R-curve behavior in toughened silicon nitride by stable crack propagation in bending. *J. Am. Ceram. Soc.*, 1995, **78**(11), 3113–3116.
14. Nishida, T., Hanaki, Y. and Pezzotti, G., Effect of notch-root radius on the fracture toughness of a fine-grained alumina. *J. Am. Ceram. Soc.*, 1995, **77**(2), 606–608.
15. Grabner, L., Spectroscopy technique for the measurement of residual stress in sintered Al_2O_3. *J. Appl. Phys*, 1978, **49**(2), 580–583.
16. Muraki, N., Sergo, V., Pezzotti, G., Katagiri, G., Meriani, S. and Nishida, N., Raman piezo-spectroscopic behavior of aluminum nitride. *Applied Spectrosc.*, 1997, **51**(11), 1761–1765.
17. Ravichandran, S., The mechanics of toughness development in ductile phase reinforced brittle matrix composites. *Acta Metall. Mater.*, 1992, **40**(5), 1009–1022.
18. Kotoul, M., On the shielding effect of a multiligament zone of a crack in WC–Co. *Acta Metall. Mater.*, 1997, **45**(8), 3363–3376.
19. Swearengen, J.C., Beauchamp, E.K. and Eagan, R.J., Fracture toughness of reinforced glasses. In *Fracture Mechanics of Ceramics*, Vol. 4. Plenum Press, New York, 1978, pp. 973–987.
20. Virkar, A. V. and Johnson, D. L., Fracture behaviour of ZrO_2–Zr composites. *J. Amer. Ceram. Soc.*, 1977, **60**(11-12), 514–519.
21. Mori, T. and Tanaka, K., Average stress in matrix and average energy of materials with misfitting inclusions. *Acta metall*, 1973, **21**, 571–574.
22. Taya, M., Hayashi, S., Kobayashi, A. S. and Yoon, H. S., Toughening of a particulate-reinforced ceramic-matrix composite by thermal residual stress. *J. Am. Ceram. Soc.*, 1990, **73**(5), 1382–1391.
23. Underwood, E. E., In *Quantitative Stereology*. Addison-Wesley Publ., Reading, MA, 1970.
24. Irwin, G. R., Fracture. In *Handbuch der Physik*, Vol. 6. Springer-Verlag, Berlin, 1958, pp. 551–594.